land

MDPI

Article

Spatiotemporal Variation and Driving Mechanisms of the Global Production-Living-Ecological Space Coupling Coordination Degree

Weisong Li [1,2,3], Yi Zeng [4], Yelin Peng [4], Wanxu Chen [4,*], Ying Dong [5], Ziyan Ye [6] and Yan Chen [7]

1 Hubei Key Laboratory of Digital Finance Innovation, Hubei University of Economics, Wuhan 430205, China; lws@hbue.edu.cn
2 Collaborative Innovation Center for Emissions Trading System Co-Constructed by the Province and Ministry, Wuhan 430205, China
3 Experimental Teaching Center, Hubei University of Economics, Wuhan 430205, China
4 Department of Geography, School of Geography and Information Engineering, China University of Geosciences, Wuhan 430078, China; zy415@cug.edu.cn (Y.Z.); 20211003202@cug.edu.cn (Y.P.)
5 Interdisciplinary Research Institute in New Finance and Economics, School of Digital Economics, Hubei University of Economics, Wuhan 430205, China; dongying@hbue.edu.cn
6 Faculty of Accounting, Hubei University of Economics, Wuhan 430205, China; 22050200@email.hbue.edu.cn
7 School of Computer Science, China University of Geosciences, Wuhan 430074, China; 20221002134@cug.edu.cn
* Correspondence: cugcwx@cug.edu.cn

Abstract: The coupling coordination degree (CCD) of the production-living-ecological space (PLES) functional index is an indicator of regional sustainable development potential. However, previous studies have failed to reveal the driving mechanisms of the CCD of PLES functional index on a global scale. Therefore, this study employed the CCD model to evaluate the CCD of the PLES functional index and spatial regression models to measure the heterogeneous drivers using multi-source data in 2000, 2010, and 2020. The results demonstrated that ecological spaces dominated (85%) globally, while living spaces comprised the smallest share (3%). The ecological functional index was higher than the production and living functional indices. Further analyses revealed that topographic factors were the main restricting factors for PLES; the proportion of production and living spaces decreased with increasing altitude and slope, whereas ecological spaces showed the opposite trend. The global CCD values of the PLES functional index in 2000, 2010, and 2020 were 0.186, 0.189, and 0.198, respectively, showing an increasing trend. High CCD was generally observed in areas with dense population and industry where human activity systems interact with natural ecosystems. The formation of the CCD of the global PLES functional pattern results from the joint action of natural and socioeconomic factors, with pronounced spatial heterogeneity. Our findings can help optimize global territorial space utilization, improve territorial space utilization efficiency, and realize global sustainable development goals.

Keywords: PLES; spatiotemporal pattern; CCD; driving forces; geographically weighted regression; global

check for updates

Citation: Li, W.; Zeng, Y.; Peng, Y.; Chen, W.; Dong, Y.; Ye, Z.; Chen, Y. Spatiotemporal Variation and Driving Mechanisms of the Global Production-Living-Ecological Space Coupling Coordination Degree. *Land* **2024**, *13*, 2136. https://doi.org/10.3390/land13122136

Academic Editor: Charlie Shackleton

Received: 15 October 2024
Revised: 21 November 2024
Accepted: 2 December 2024
Published: 9 December 2024

Copyright: © 2024 by the authors. Licensee MDPI, Basel, Switzerland. This article is an open access article distributed under the terms and conditions of the Creative Commons Attribution (CC BY) license (https://creativecommons.org/licenses/by/4.0/).

1. Introduction

The concept of production-living-ecological space (PLES), covering the dimensions of ecological space (ES), production space (PS), and living space (LS), encompasses the spatial activities of material production and the spiritual life of human beings. PLES constitutes the appearance of the world in which human beings live and perform activities and utilize natural resources. It is a complex space system with multi-element interaction and multiscale space nesting [1]. ES, PS, and LS are interdependent and influence each other, constituting the cornerstone of regional sustainable development. The coordination and balance among them are directly related to the sustainable development capacity of the

region and human well-being [2]. Thus, PLES is the primary means through which humans survive and develop and is an indispensable vehicle for socioeconomic advancement.

The phenomenon of rapid urbanization has given rise to numerous challenges pertaining to the realization of sustainable development. These include the absence of a concentration of PS, the low efficiency and poor quality of LS, and the lack of protection afforded to ES [2,3]. The accelerated pace of global urbanization has resulted in a significant increase in the impact of human activities on the natural environment. This has led to an urgent need to address the balance and coordination among PLES. Considering these issues, realizing the functional coupling coordination degree (CCD) of PLES on a global scale has become the focus in several disciplines, including urban planning, environmental science, and economics [3]. As the concept of sustainable development has evolved from global to local action, the capacity of PLES to adapt to complex eco-environmental changes and meet the growing material requirements of humans has become a significant challenge [4]. Revealing the CCD among the functional indices of PLES and its influencing factors is vital to forming a powerful and efficient PS, a livable and moderately sized LS, and an effective ES. This has significant theoretical and practical implications for optimizing territorial space, developing an ecological civilization, and promoting sustainable development. Previous studies have focused on the theoretical connotation and conceptual framework of territorial space [5], the classification and identification of PLES [6–11], and the evolution of PLES in terms of its spatiotemporal characteristics [12–18]. In addition, the spatiotemporal evolution of PLES and its influencing factors [19] and its optimization [20–26] have been significant areas of investigation. The eco-environmental effects of PLES are another research hotspot [22–27]. For instance, studies have determined ecosystem services from the perspective of PLES, explained the spatiotemporal response of ecosystem services to PLES changes [25,28], and measured eco-environmental effects with the help of the eco-environment quality index [20,29–31]. Furthermore, studies have conducted multifunctional evaluations of PLES, assessed its degree of spatial sustainable development [22,23], investigated the regulation and optimization of PLES conflict [32–34], and determined its utilization efficiency [32–35].

The spatial pattern of territorial space is transforming from dominant PS to the coordinated development of PLES. Previous studies on the CCD of PLES functions [2,31,36,37] and planning practices of national spatial multifunctionality [3,38] have significantly contributed to the field through extensive research and exploration. Methods for evaluating the spatial function of PLES include multi-index evaluation [32,39] and expert assignment [14]. Previous research has demonstrated that the intricate interdependencies among the PLES functional index, characterized by mutual facilitation and mutual coercion, exert a profound influence on the evolution of territorial space [2,37,40], with the overdevelopment of one function of PLES influencing the execution of other functions within the system. Furthermore, spatiotemporal characteristics vary depending on the differences in socioeconomic development and the geographical environment at distinct stages [13,18]. Globally, different countries and regions exhibit significant differences in the functional division, utilization, and management modes of PLES. Some developed countries have realized the efficient utilization and coordinated development of PLES through advanced planning concepts and technical means. However, developing countries face multiple challenges, such as resource shortages, environmental pollution, and ecological degradation, and the CCD of PLES functions is low [8]. Therefore, exploring the coupling and interaction among the roles of PLES and clarifying its spatiotemporal evolution rules and driving factors can contribute to coordinating the contradiction among the allocation of the resources of PLES, realizing the integration and coordinated development of the functions of PLES, and informing theoretical means for clarifying the direction of regional development and guiding sustainable development.

Previous studies employed the CCD model to reveal the CCD relationship of multiscale PLES and the CCD relationship among the functions of PLES [2,31,37,41]. Transformations in the CCD of the PLES functional index are not solely confined to the ecological

domain, they may also exert considerably influence on social structures and economic activities. Particularly, an increase in the CCD of PLES contributes to the sustainability of regional development, resulting in a more rational allocation of resources and an overall enhancement in the regional socioeconomic development [42]. Additionally, the changes may also lead to the redistribution of human social groups [43] and exert an influence on agricultural production and the urbanization process, thus having direct and indirect effects on the regional economy [44]. PLES is affected by the comprehensive effects of resources, environment, and socioeconomic factors [19,45–47]. However, the variability of the spatiotemporal characteristics of PLES and the exact mechanism of CCD formation remains elusive. Previous study of PLES mainly focus on microscales such as counties and townships, but lacks a global perspective [38,48]. To fill this gap, we aimed to identify the mechanisms driving the heterogeneity of CCD among PLES functions at the global scale.

Since the beginning of the 21st century, global PLES has undergone a profound restructuring of its spatial pattern, form, and eco-environment as a result of economic transformation and upgrading driven by globalization and information technology, as well as the interactive reorganization of social factors. Despite the extensive research conducted on PLES at various scales, few studies have investigated CCD among the functional indices of PLES and its underlying drivers on a global scale. Therefore, this study aimed to (1) map global PLES functions, (2) measure the CCD of global PLES functions, and (3) reveal the driving factors of the CCD of the global PLES function index using a geographically weighted regression (GWR) model. Research on the CCD of the global PLES functional index can provide a scientific basis and reference for global territorial space optimization. According to the actual situation and development needs of different regions, planners can scientifically and reasonably divide the functional layout of PLES to promote the coordinated development of the economy, society, and ecology.

2. Materials and Methods

2.1. Data Sources and Processing

The PLES datasets used in this study were obtained from Fu et al. [8], who combined global land cover data for 2000, 2010, and 2020 obtained by Globe Land30 with the population density data provided by the Center for Socioeconomic Data and Applications of NASA to construct a global PLES dataset. The dataset provides data support for global territorial space research and provides an essential reference for assessing the coordinated development of the SDGs. The impact factor data involved in the driver analysis of the CCD of the PLES functions included the average annual precipitation, altitude, proportion of forest, nighttime light density, and road density. Specifically, the average annual precipitation data were obtained from the CHIRPS Pentad dataset, Climate Hazards Group InfraRed Precipitation with Station Data, and processed using the Google Earth Engine. The altitude data were downloaded from the Shuttle Radar Topography Mission (https://earthexplorer.usgs.gov/ (accessed on 26 November 2024)). The proportion of forest was derived from the European Space Agency and Climate Change Initiative (ESA-CCI). Nighttime light and road density data were obtained from the National Earth System Science Data Center, National Science & Technology Infrastructure of China (http://www.geodata.cn (accessed on 26 November 2024)), and NASA Socioeconomic Data and Applications Center (https://sedac.ciesin.columbia.edu/ (accessed on 26 November 2024)), respectively. We obtained global county-level shape-file data for subdistrict statistics from the most recent global administrative area database (https://gadm.org/ (accessed on 26 November 2024)).

2.2. PLES Index Measurement

The division of PLES is mainly based on land use functions, involving the three dimensions LS, PS, and ES. The differentiation of land use functions is mainly based on land use types, and the classification system of PLES reflects this. Transitions in land use are frequently characterized by shifts in dominant functions, particularly the transformation

among three primary functions [28,49]. A substantial body of research has been conducted on the classification of territorial space [50]. This study drew on Cui et al. (2022), Wang et al. (2022), and expert knowledge to quantify the various functions provided by different territorial spaces (Table 1) [14,28,45,51,52]. The method allows for a quick and accurate assessment of the type and intensity of land use functions. The equations used for the calculations are as follows:

$$PSI = \left(\sum_{i=1}^{n} LA_{i,t} \times PS'_{i,t}\right) \Big/ \sum_{i=1}^{n} LA_{i,t}, \quad (1)$$

$$LSI = \left(\sum_{i=1}^{n} LA_{i,t} \times LS'_{i,t}\right) \Big/ \sum_{i=1}^{n} LA_{i,t}, \quad (2)$$

$$ESI = \left(\sum_{i=1}^{n} LA_{i,t} \times ES'_{i,t}\right) \Big/ \sum_{i=1}^{n} LA_{i,t}, \quad (3)$$

where PSI is the functional index of PS, LSI is the functional index of LS, and ESI is the functional index of ES. PS', LS', and ES' are respectively the function scores of PLES. $LA_{i,t}$ is the area of the i-th land-use type and n is the number of territorial space types in the secondary category of this study.

Table 1. PLES classification and its function scoring.

Primary Category	Secondary Category	PS Function Scoring	LS Function Scoring	ES Function Scoring
PS	Agricultural PS	3	0	3
	Industrial PS	5	1	0
LS	Urban LS	3	5	0
	Rural LS	3	5	0
ES	Forest ES	1	0	5
	Grassland ES	1	0	5
	Water ES	1	0	5
	Other ES	0	0	3

2.3. Standard Deviation Ellipse Method

The standard deviation ellipse method is a classic method for analyzing the directional characteristics of spatial distribution. It analyzes the spatial structural characteristics of geographic data by calculating the spatial standard deviation of geographic elements and forming an ellipse-shaped distribution map. Furthermore, it can intuitively reveal the spatial characteristics of geographic elements, including center, dispersion, and directional trends. In ArcGIS 10.4, a series of tools are available to visualize the standard deviation ellipse [53]. In this study, a standard deviation ellipse was used to identify the spatiotemporal evolution trend in global PLES. The calculation equations are as follows:

$$\overline{X}_w = \sum_{i=1}^{n} w_i x_i \Big/ \sum_{i=1}^{n} w_i \quad (4)$$

$$\overline{Y}_w = \sum_{i=1}^{n} w_i y_i \Big/ \sum_{i=1}^{n} w_i \quad (5)$$

$$\theta = \arctan\left[\left(\sum_{i=1}^{n} x_i'^2 - \sum_{i=1}^{n} y_i'^2\right) + \sqrt{\left(\sum_{i=1}^{n} x_i'^2 - \sum_{i=1}^{n} y_i'^2\right)^2 + 4\left(\sum_{i=1}^{n} x_i' y_i'\right)^2}\right] \Big/ 2\sum_{i=1}^{n} x_i' y_i', \quad (6)$$

$$\delta_x = \sqrt{\sum_{i=1}^{n}\left(x_i' \cos\theta - y_i' \sin\theta\right)^2 \Big/ n}, \delta_y = \sqrt{\sum_{i=1}^{n}\left(x_i' \sin\theta - y_i' \cos\theta\right)^2 \Big/ n}, \quad (7)$$

where $(\overline{X}_w, \overline{Y}_w)$ is the weighted average center of PLES; (x_i, y_i) is the geometric center coordinate of unit i; w_i and θ represent weights and azimuths, respectively; and δ_x and δ_y are the standard deviation along the major and minor axes, respectively.

2.4. CCD Model

As a significant component of the national space, PLES fulfills the roles of economic production, human life, and natural ecology. The CCD of the PLES functional index pertains to the interdependence and advancement of PLES through the circulation of resources, the exchange of information, and the transmission of energy, to attain the most significant overall benefit. This process not only requires the optimization of the internal functions of each space, but also emphasizes the coordination and complementarity of PLES. The CCD model reflects the phenomenon of synergy between two or more geographical elements through interactions and mutual influences [54]. The CCD model combines the degrees of coupling and coordination to obtain a comprehensive evaluation indicator, which aids in comprehensively assessing the level of coordinated development of the system. Notably, a high degree of coupling does not necessarily imply a high overall system benefit. The development level of the coupling relationship between the elements must also be considered, namely whether coordination has been achieved [45]. Based on the physical model, the CCD model of the PLES functional index was constructed as follows:

$$C = \left\{ P(g) \cdot L(l) \cdot E(e) \Big/ \left((P(g) + L(l) + E(e)/3)^3 \right) \right\}^{1/3} \quad (8)$$

The coupling degree C can only represent the strength of the interaction and influence among the PLES functional indices and cannot reflect the synergistic development among the PLES functional indices. Accordingly, CCD model D is an appropriate means of reflecting the synergistic development among the PLES functional indices. The calculation equations are as follows:

$$T = \alpha P(p) + \beta L(l) + \lambda E(e) \quad (9)$$

$$D = \sqrt{T \cdot C} \quad (10)$$

where T is the coordination index, and α, β, and λ are the undetermined coefficients. Considering that PLES has the same key role in the development of territorial space, and $\alpha + \beta + \lambda = 1$, the values were set to $\alpha = \beta = \lambda = 1/3$. The CCD of the PLES functional index is divided into the following five categories—severe recession disorder zone (0–0.20), moderate recession disorder zone (0.21–0.40), barely coupled harmonized zone (0.41–0.60), positive coupled harmonized zone (0.61–0.80), and high-quality coupled harmonized zone (0.81–1).

2.5. Spatial Autocorrelation Analysis

Global and local spatial autocorrelation methods are frequently employed in exploratory spatial data analysis to elucidate both the global and local clustering patterns of geographical elements [55]. Global spatial autocorrelation describes the spatial characteristics of attribute values across an entire region. By calculating various indices, this method assesses the overall spatial autocorrelation and degree of spatial variation, thereby measuring the spatial agglomeration of the global CCD of the PLES functional index. The equation used for the calculations is as follows:

$$I = \frac{n\sum_{i=1}^{n}\sum_{i=1}^{n}\omega_{ij}(x_i-\overline{x})(x_j-\overline{x})}{\sum_{i=1}^{n}\sum_{i=1}^{n}\omega_{ij}\sum_{i=1}^{n}(x_i-\overline{x})^2} \quad (11)$$

where ω_{ij} is the spatial weight matrix, n is the number of regional units, x_i is the observed value of the i-th unit, and $\overline{x}$ is the mean value of the observations.

The local spatial association reveals the heterogeneity of spatial differences to fully reflect the changing trends of regional spatial differences, which can further reveal the spatial differences in the CCD of the global PLES functional index. The equation used for the calculations is as follows:

$$I_i = \frac{x_i-\overline{X}}{S_i^2}\sum_{j=1,i\neq j}^{n}\omega_{ij}(x_j-\overline{X}) \quad (12)$$

where $S^2{}_i$ is the variance of the attribute value x_i, and I_i is the local spatial autocorrelation index.

2.6. Geographically Weighted Regression

To determine the spatial heterogeneity of the factors influencing the CCD of the PLES functional index, we employed the GWR model [56]. GWR, an extension of the ordinary least squares (OLS) regression model, incorporates the geographic location of data into the regression parameters, allowing for the local estimation of these parameters, thus revealing spatial non-stationarity in the influencing factors. The GWR model is calculated as follows:

$$y_i = \beta_0(m_i,n_i) + \sum_{j=1}^{k}\beta_j(m_i,n_i)x_{ij} + \varepsilon_i \quad (13)$$

where x_{ij} is the observed value of the j-th variable in the i-th sample space unit, and (m_i, n_i) is the geographical location coordinate of the i-th sample space unit.

The PLES spatial pattern is a regional complex formed by long-term interactions among human production, construction activities, and the natural geographical environment [56]. The natural environment and socioeconomic factors jointly influence the CCD of the PLES function index [2,50]. Concerning the former, previous studies have demonstrated that climate factors play a pivotal role in determining the spatiotemporal characteristics of PLES, with climate elements exerting a discernible impact on the function of PLES [14]. The mean annual precipitation was selected as the climatic factor for the analysis. Furthermore, the topographic factors shaping the Earth's surface landscape are closely related to the CCD of the PLES functional index. In this study, the altitude was selected as a representative topographic factor. For example, plains are suitable for agricultural production, whereas mountainous and hilly areas are more suitable for ecological protection. The type of land cover, specifically forest, has a significant impact on the CCD of the PLES functional index. Socioeconomic factors, such as economic development level, population distribution, and economic policies, also play a decisive role in PLES distribution. Economically developed areas often have more PS and LS, but also pay more attention to the protection of ES. Densely populated areas require more LS, and cultural traditions and religious beliefs may affect people's cognition and attitudes toward ES. For socioeconomic factors, road density and nighttime light density were selected for characterization [50].

3. Results

3.1. Spatiotemporal Patterns of Global PLES from 2000 to 2020

The proportions of PS at the county level in 2000, 2010, and 2020 were 11.625%, 11.702%, and 12.191%, respectively (Figure 1), indicating a clear trend of continuous increase. Spatially, PS was primarily distributed in most parts of Europe and Asia, including the southern parts of India, northeastern parts of China, and parts of Myanmar and Thai-

land. PS in Africa was generally relatively low, with only a few high areas distributed in Ethiopia, Sudan, Tanzania, and Nigeria. In South America, PS was primarily distributed in southern Brazil and northern Argentina. In North America, PS was mainly located along the Mississippi River in the United States and southern Canada. The high PS areas in Australia were distributed in the southeastern and southwestern regions of Australia.

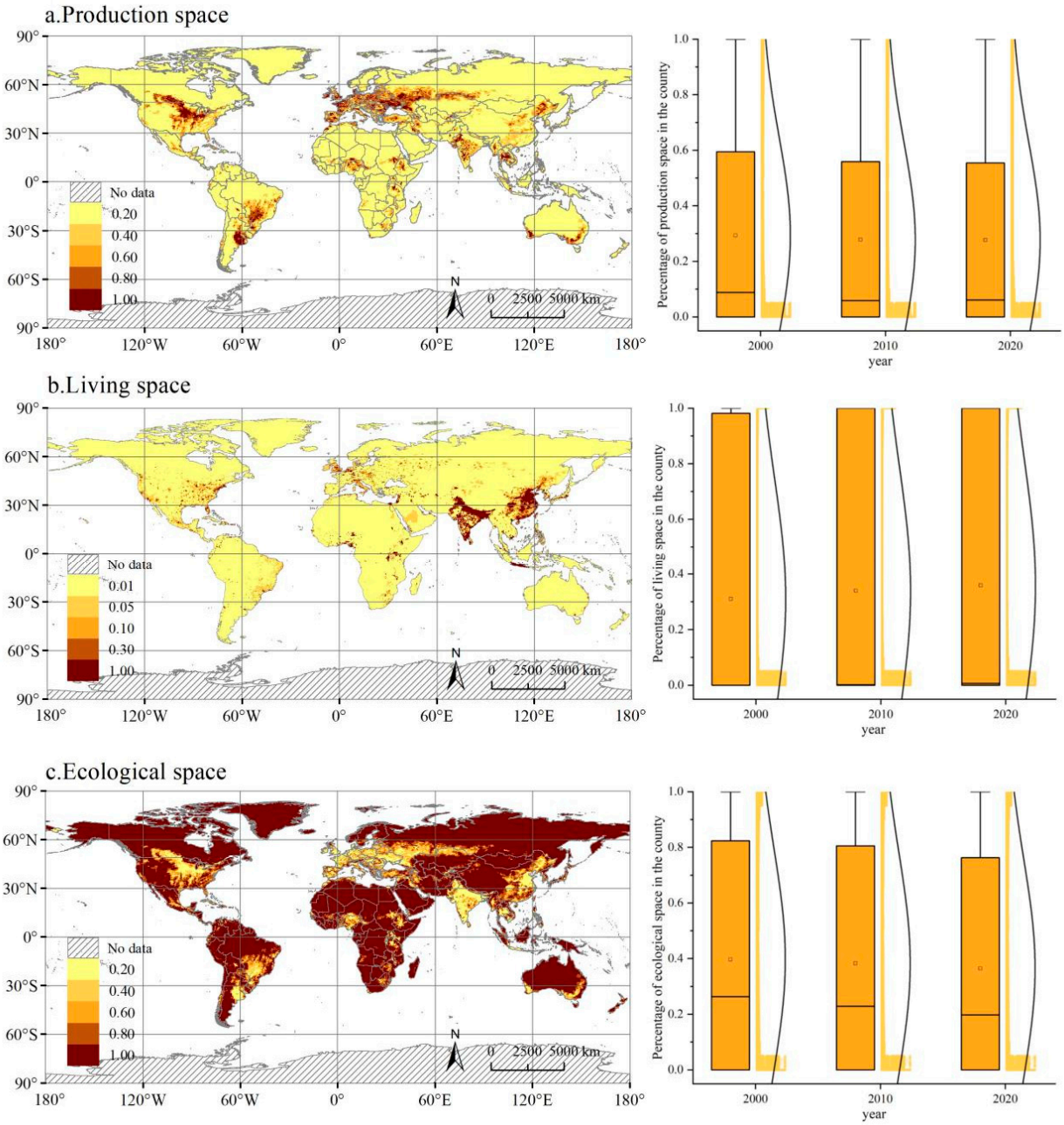


Figure 1. Spatial patterns of global PLES.

The proportions of LS at the county level in 2000, 2010, and 2020 were 2.550%, 2.839%, and 3.116%, respectively, indicating an evident increasing trend. Globally, the distribution of LS showed evident spatial agglomeration characteristics. LS was primarily distributed in the central and eastern regions of China, India, Japan, Indonesia, and other countries. LS was mainly found in other large cities worldwide and surrounding areas such as European cities and eastern and western cities in the United States. In 2000, 2010, and 2020, the proportions of county ES were 85.825%, 85.459%, and 84.693%, respectively. Thus, the proportions of ES were the highest and LS the lowest.

Worldwide, 74.512% of the territorial space was distributed in the area below 500 m, the territorial space of 500–1000 m accounted for 14.819%, the territorial space of 1000–1500 m accounted for 7.612%, and the territorial space of 1500–2000 m accounted for 4.161% (Figure 2). The proportion of territorial space within 2000–4000 m was 5.083%, and the proportion of territorial space above 4000 m was 0.849%. The variation in PLES was evident at different altitudes.

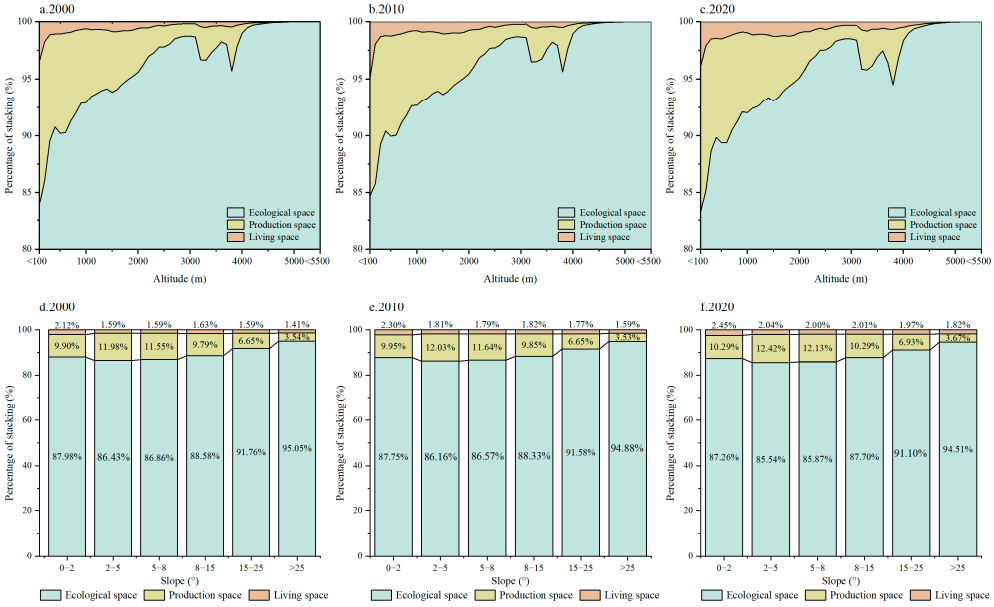


Figure 2. Changes in the proportion of global PLES at different altitudes and slopes in 2000, 2010, and 2020. (**a**–**c**) are the stacking percentage of PLES at different altitudes in 2000, 2010, and 2020, respectively. (**d**–**f**) are the stacking percentage of PLES at different slopes in 2000, 2010, and 2020, respectively.

With respect to ES, the proportion of ES generally showed an increasing trend with an increase in altitude but decreased in the range of 500–600 m and 3000–4000 m. The proportions of ES below 1000 m in 2000, 2010, and 2020 were 84.142%, 82.314%, and 84.088%; from 1000 to 2000 m were 11.707%, 13.048%, and 11.722%; from 2000 to 3000 m were 4.969%, 5.546%, and 5.002%; and above 3000 m were 1.885%, 2.105%, and 1.897%, respectively.

The proportion of LS decreased gradually with increasing altitude. Specifically, in 2000, 2010, and 2020, the proportions of LS below 500 m were 90.161%, 92.165%, and 90.195%; from 500 to 1000 m were 4.656%, 4.058%, and 4.914%; from 1000 to 2000 m were 4.107%, 3.045%, and 3.951%; and above 2000 m were 1.076%, 0.731%, and 0.940%, respectively. In general, PS also decreased evidently with an increase in altitude, but there was an apparent increase between 3000 and 4000 m. Specifically, the proportions of PS below an altitude of 500 m were 85.827%, 86.404%, and 83.557%; from 500 to 1000 m were 8.450%, 8.105%, and 9.804%; from 1000 to 2000 m were 4.828%, 4.622%, and 5.596%; and above 2000 m were 0.894%, 0.869%, and 1.043%, respectively.

With an increase in slope, the ES demonstrated a trend of first decreasing and then increasing, only decreasing from 0–2° to 2–5°. In general, the proportion of ES in different slope ranges in 2000, 2010, and 2020 decreased. For example, within the range of >25° in 2000, 2010, and 2020, the proportions of ES were 95.05%, 94.88%, and 94.51%, respectively. In contrast, the proportions of PS and LS increased gradually with an increasing slope. Specifically, the proportion of PS initially increased and then decreased as the slope increased. The proportion of PS increased from 0–2° to 2–5° and then continued to decrease with increasing slope. The proportions of PS were 3.540%, 3.530%, and 3.670% in the range of >25° in 2000, 2010, and 2020, respectively. The proportion of LS was the lowest in different slope ranges and demonstrated a decreasing trend with the increase in slope, increasing

between 5–8° and 8–15° and then decreasing continuously. In 2000, 2010, and 2020, the proportions of LS in the range of >25° were 1.410%, 1.590%, and 1.820%, respectively.

This study plotted the standard deviation ellipse of the global PLES in 2000, 2010, and 2020 to reveal its evolutionary trend (Figures 3 and 4). In general, the global PLES formed an east-west spatial distribution pattern. The standard deviation ellipse of the global PLES increased in the *X*-axis direction more than in the *Y*-axis direction, indicating that PLES expanded along the *X*-axis direction, that is, in the east-west direction. The gravity center of PLES was in the northern hemisphere, with those of PS and ES in the eastern hemisphere and those of LS in the western hemisphere. From 2000 to 2010, the gravity center of the PS shifted 50.803 km to the northwest, and from 2010 to 2020, it shifted 48.318 km to the northwest (Table 2). The PS advanced in a northwest direction during the study period.

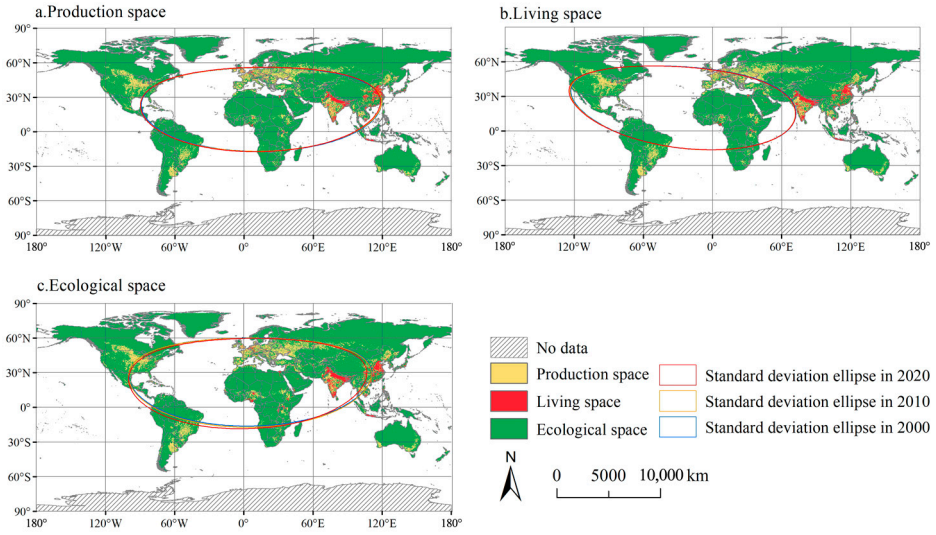


Figure 3. Standard deviation ellipse of global PLES pattern from 2000 to 2020.

The area of the standard deviation ellipse for the LS increased, with more pronounced growth along the *X*-axis than along the *Y*-axis, indicating a notable expansion of the LS in the west-east direction. The gravity center for LS shifted 61.106 km southwest from 2000 to 2010 and 39.383 km northwest from 2010 to 2020. In addition, the ellipse of deviation for ES experienced a southwesterly shift of 63.558 km from 2000 to 2010 and a significant shift of 276.863 km from 2010 to 2020.

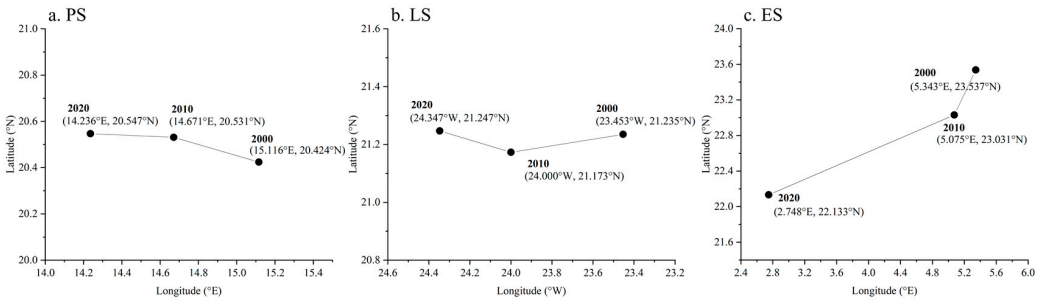


Figure 4. Gravity center shift in PLES from 2000 to 2020.

Table 2. Standard deviation ellipse parameter of global PLES from 2000 to 2020.

	Year	Center (X, Y)	Xstd Dist (km)	Ystd Dist (km)	Rotation
PS	2000	15.116° E, 20.424° N	11,607.072	4664.199	89.329
	2010	14.671° E, 20.531° N	11,654.280	4674.982	88.941
	2020	14.236° E, 20.547° N	11,594.227	4723.210	88.805
LS	2000	23.453° W, 21.235° N	10,949.936	4542.532	97.518
	2010	24.000° W, 21.173° N	10,958.921	4527.223	97.597
	2020	24.347° W, 21.247° N	11,025.622	4514.245	97.577
ES	2000	5.343° E, 23.537° N	11,729.651	5114.636	89.223
	2010	5.075° E, 23.031° N	11,726.526	5161.597	89.257
	2020	2.748° E, 22.133° N	11,506.109	5183.886	87.963

To reveal the transfer characteristics among PLES, a Sankey map was drawn to visualize the transfer matrix during the periods 2000–2010 and 2010–2020 (Figure 5). The conversion between global forest ES and grassland ES from 2000 to 2010 was the most intense, with 25.171 × 10^6 km^2 of forest ES converted to grassland ES. Simultaneously, 16.167 × 10^6 km^2 of grassland ES was transformed into forest ES. In addition, the conversion between other terrestrial spaces and forest ES and grassland ES was relatively strong due to the large area of ES on a global scale. From 2000 to 2010, the amount of agricultural PS converted into LS was much higher than the amount of LS converted to agricultural PS. Specifically, from 2000 to 2010, 21 km^2 and 1.424 × 10^5 km^2 of urban and rural LS, respectively, were transformed into PS. In contrast, 206 km^2 and 1.384 × 10^6 km^2 of agricultural PS were transformed into urban and rural LS, respectively.

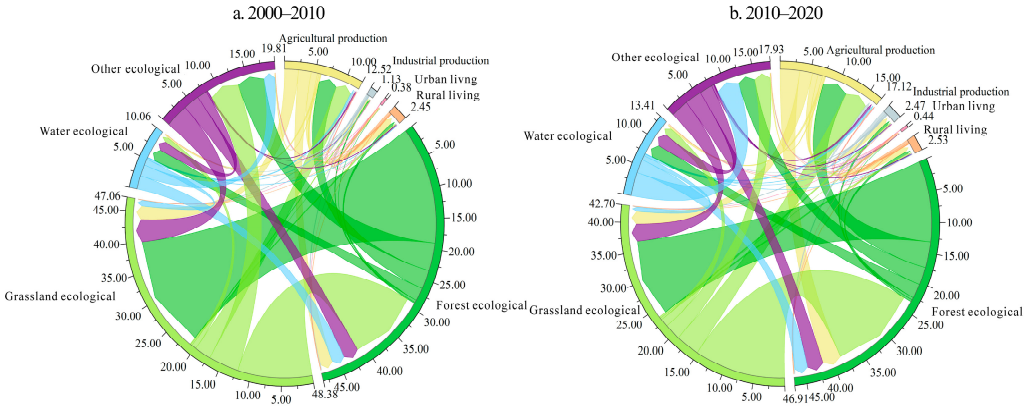


Figure 5. Sankey diagram of land-use transfer matrix (unit: ×10^6 km^2).

Similarly, the shift between global forest ES and grassland ES was the strongest between 2010 and 2020; 13.125 × 10^6 km^2 of forest ES was transformed into grassland ES. Simultaneously, 15.084 × 10^6 km^2 of grassland ES was converted to forest ES. Similarly, the transition between ES and other spaces was also strong. The disparity between the amount of agricultural PS converted into LS and the amount of LS converted into agricultural PS was more evident from 2010 to 2020. Specifically, 48 km^2 and 1.569 × 10^5 km^2 of urban and rural LS were transformed into agricultural PS from 2010 to 2020, respectively. In contrast, 5217 km^2 and 9.395 × 10^5 km^2 of agricultural PS were transformed into urban and rural LS, respectively. Compared with the previous decade, the occupation of agricultural PS by urban LS increased.

3.2. Spatiotemporal Patterns of Global PLES Functional Index from 2000 to 2020

In 2000, 2010, and 2020, the global PSI was 2.199, 2.227, and 2.267; the LSI was 1.544, 1.692, and 1.788; and the ESI was 2.762, 2.650, and 2.546, respectively. In general, we

found that the global PSI and LSI demonstrated a slow-increasing trend. ESI, on the contrary, showed a slow decline. In terms of spatial distribution, we can find that the spatial distribution characteristics of PSI, LSI, and ESI were consistent with those of PS, LS, and ES (Figures 6–8).

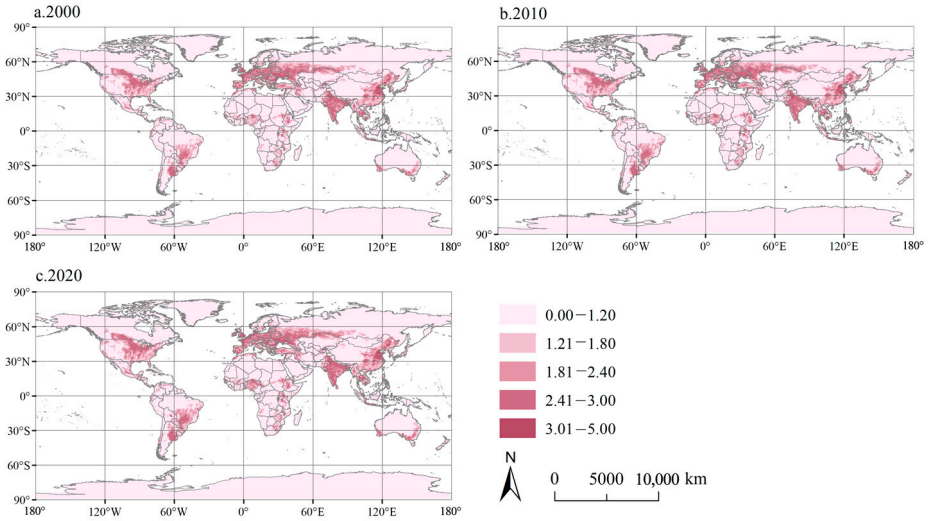


Figure 6. Spatiotemporal patterns of global PSI from 2000 to 2020.

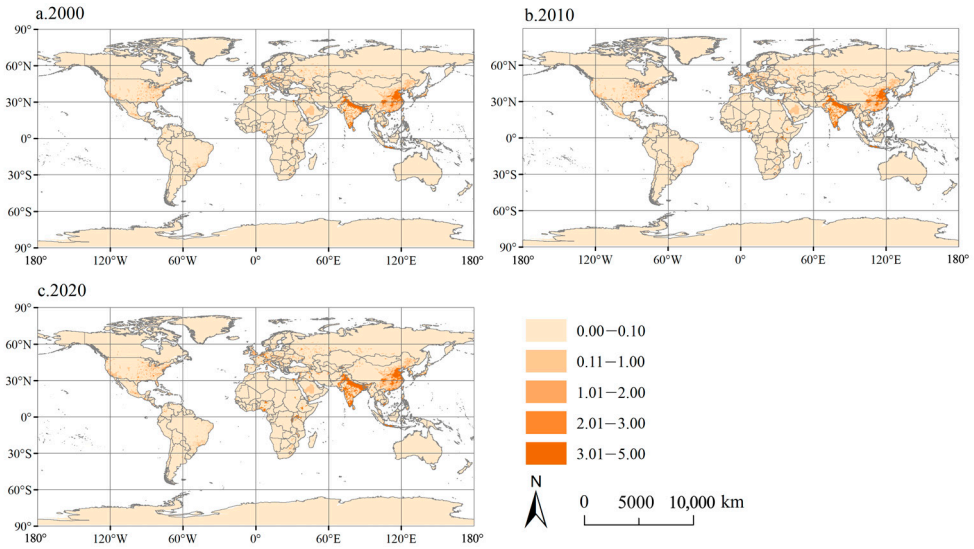


Figure 7. Spatiotemporal patterns of global LSI from 2000 to 2020.

PS is a space for the provision of agricultural products or services for human beings, distributed in major agricultural regions and industrial, mining, and transportation construction land, including central and eastern China, India, most parts of Europe, and the Mississippi River Valley in the United States. LS is closely related to population distribution and is primarily concentrated in high-density population areas (e.g., plain areas, urban agglomerations, key cities, and surrounding areas). ES mainly included forest, grassland, water areas, and unused land, which was primarily distributed in mountainous and desert areas.

3.3. CCD of Global PLES Functional Index from 2000 to 2020

Figure 9 presents the CCD of the global PLES functional index from 2000 to 2020. In 2000, 2010, and 2020, the CCD of the global PLES functional index was 0.186, 0.189, and 0.198, respectively. Spatially, the severe recession disorder zone occupied the leading

position at 58.194%, 57.584%, and 55.047% in 2000, 2010, and 2020, respectively. This was followed by moderate recession disorder zones at 19.091%, 19.204%, and 21.016% in 2000, 2010, and 2020, respectively. Barely coupled harmonized zones accounted for 16.061%, 16.392%, and 17.223% in 2000, 2010, and 2020, respectively. The number of positively coupled harmonized zone types was the lowest at 6.654%, 6.819%, and 6.714% in 2000, 2010, and 2020, respectively. There were no high-quality coupled harmonization types. The positively coupled harmonized zone type was primarily distributed in China's Sichuan Basin and the middle and lower reaches of the Yangtze River plain, as well as in some large cities in India, North America, Europe, and other regions. The poorly coupled harmonized zone was scattered across the area surrounding the positively coupled harmonized zone. These two areas were concentrated in the PS and LS. Generally, the CCD of the PLES functional index was relatively high in these regions. In the surrounding areas, the ES function was superior to the function, which reduced the CCD of the PLES functional index. ES functions dominated the severe recession disorder type.

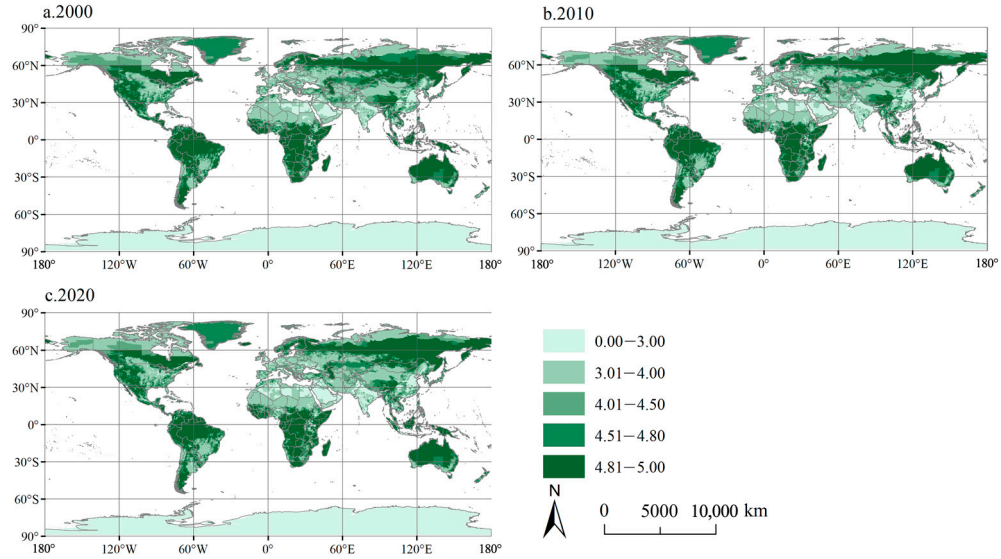


Figure 8. Spatiotemporal patterns of global ESI from 2000 to 2020.

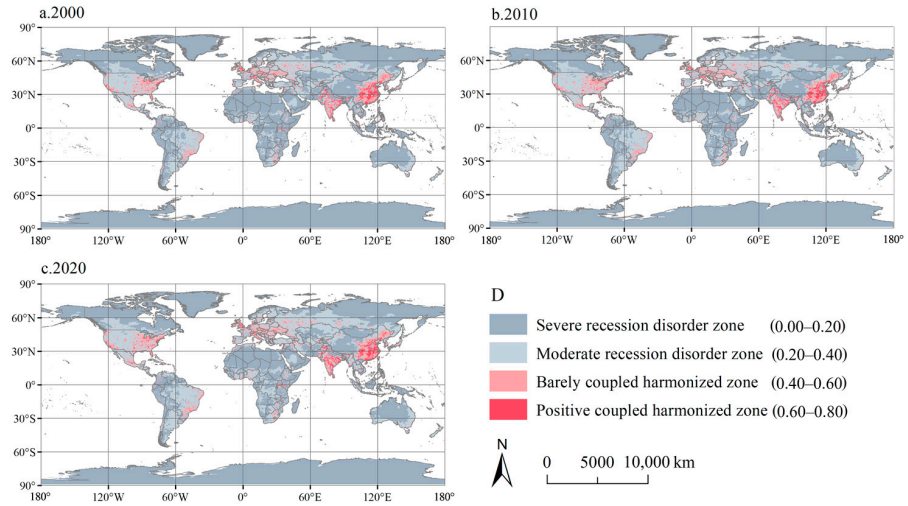


Figure 9. CCD of the global PLES functional index from 2000 to 2020.

3.4. Spatial Autocorrelation Analysis of the CCD of the Global PLES Functional Index from 2000 to 2020

The global spatial autocorrelation indices of the CCD of the global PLES functional index in 2000, 2010, and 2020 were 0.562, 0.567, and 0.569, respectively (Figure 10), with

p-values being significant at the 0.001 level and z-values of 526.919, 524.695, and 558.747, respectively. This shows a significant spatial dependency in the CCD of the global PLES functional index. The results of the local spatial autocorrelation showed that the functional CCD of PLES was dominated by H-H, accounting for 19.535%, 19.641%, and 19.738% in 2000, 2010, and 2020. It was primarily located in central and eastern China and parts of Japan in Asia, India, South Asia, and southern Europe, a small amount of southern Africa, the eastern and western coastal areas of the United States in North America, and the eastern region of Brazil in South America. The L-L type areas were mainly scattered across Southeast Asia, northern Africa, and other regions. The other types were relatively rare.

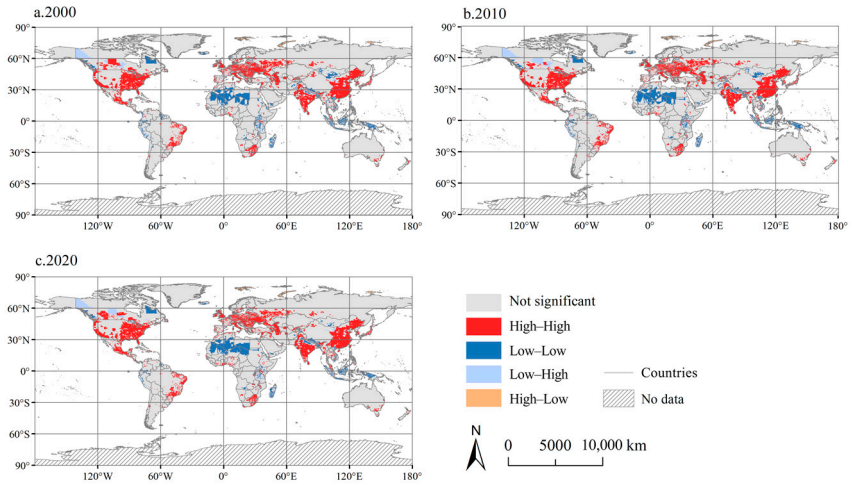


Figure 10. LISA clustering of CCD of global PLES functional index from 2000 to 2020.

3.5. Spatial Heterogeneity of the Driving Forces of CCD of PLES Functional Index from 2000 to 2020

The descriptive statistical function of SPSS was used to standardize the standard deviation of each indicator, and regression analysis was used to conduct a collinearity test on all the standardized variables. The variance inflation factors of all the variables in 2000, 2010, and 2020 were less than 3. There was no multicollinearity among the variables and the model was reasonably fitted. According to the fitting results of the OLS model, these variables can better explain the differentiation pattern of the CCD of the PLES functional index in 2000, 2010, and 2020. All the model estimates for 2000, 2010, and 2020 reached significant levels ($p < 0.01$). Among them, the overall effects of average annual precipitation, altitude, nighttime light density, and road density on the CCD of the PLES functional index were negative, with only the proportion of forest showing a significant positive effect on the CCD of the PLES functional index.

GWR model fitting was conducted for the global CCD of the PLES functional index and its influencing factors (Table 3). The model fitting degrees (adjusted R^2) for 2000, 2010, and 2020 were 0.523, 0.553, and 0.563, respectively. According to R^2, the GWR simulation results were more reasonable than the OLS simulation results. The difference in AICc between the GWR and OLS models was much more significant than 3, demonstrating that the GWR fitting results were better than those of the OLS. To compare the influence patterns of various variables on the CCD of the global PLES functional index, the fitting coefficients of the sample points in these years were statistically analyzed (Table 4).

The regression coefficients of the average annual precipitation, altitude, proportion of forest, nighttime light density, and road density are presented in Figures 11–13. The influence of the global average annual precipitation on the global CCD of the PLES functional index demonstrated evident spatial heterogeneity. The areas showing negative effects were discrete, but the contributions were significant in northern China and the Tibetan Plateau, India and South Africa. The positive effects of the annual average precipitation on the global CCD of the PLES functional index in 2000 were mainly distributed in Mongolia

in Asia, southern Russia, the Sichuan Basin in China, the North China Plain, parts of Inner Mongolia, northeastern Europe, peripheral areas of Africa, northern parts of North America, and southern parts of Australia.

Table 3. GWR model results for CCD of global PLES functional index.

Model Parameter	2000	2010	2020
Adaptive bandwidth	39	25	23
AICc	−272,172	−283,091.8	−289,556.4
R^2	0.559	0.604	0.618
Adjusted R^2	0.523	0.553	0.563

Table 4. Statistical results of GWR model coefficient values.

	Variable	X1	X2	X3	X4	X5	Intercept
2000	Min.	−73.468	−528.910	−124.530	−327,640.000	−57.464	−30.365
	1st Qu.	−0.039	−1.402	−0.108	−51.286	−0.186	0.000
	Median	0.103	0.178	−0.013	−2.871	0.379	0.144
	3rd Qu.	0.711	0.194	0.039	46.300	3.284	0.386
	Max.	168.810	813.410	48.964	4,449,800.000	49.460	19.739
2010	Min.	−111.520	−610.240	−91.120	−254,950.000	−72.862	−30.350
	1st Qu.	−0.065	−1.431	−0.112	−19.723	−0.330	0.000
	Median	0.068	−0.095	−0.004	0.000	0.132	0.119
	3rd Qu.	0.778	0.323	0.051	48.226	3.056	0.400
	Max.	90.205	815.539	5342.414	200,145.822	2570.086	22.244
2020	Min.	−207.440	−610.910	−75.745	−43,876.000	−775.050	−24.446
	1st Qu.	−0.067	−1.430	−0.114	−12.494	−0.373	0.000
	Median	0.065	−0.080	−0.003	0.000	0.092	0.128
	3rd Qu.	0.727	0.383	0.055	32.210	2.984	0.413
	Max.	170.810	651.330	2845.610	85,957.760	1832.520	

Notes: X1 denotes average annual precipitation; X2 denotes elevation; X3 denotes the proportion of forest; X4 denotes nighttime light density; X5 denotes road density.

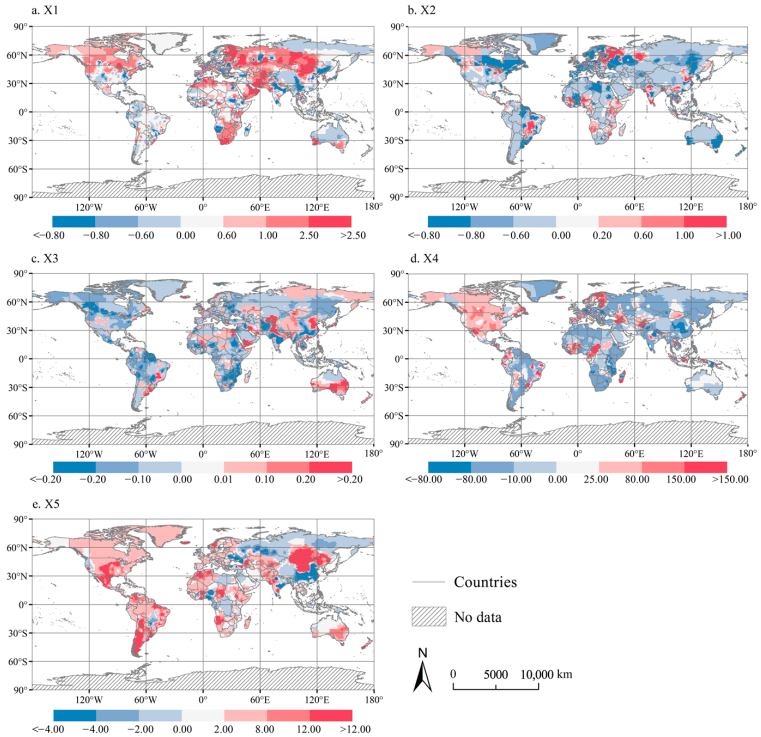


Figure 11. Coefficients of GWR model in 2000.

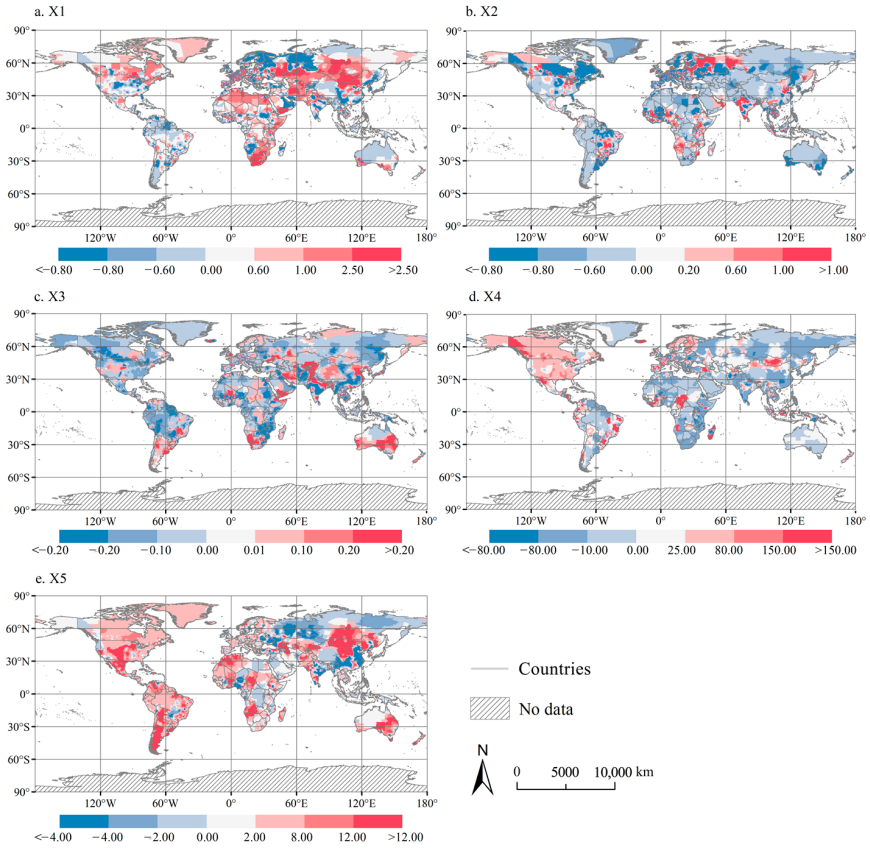


Figure 12. Coefficients of GWR model in 2010.

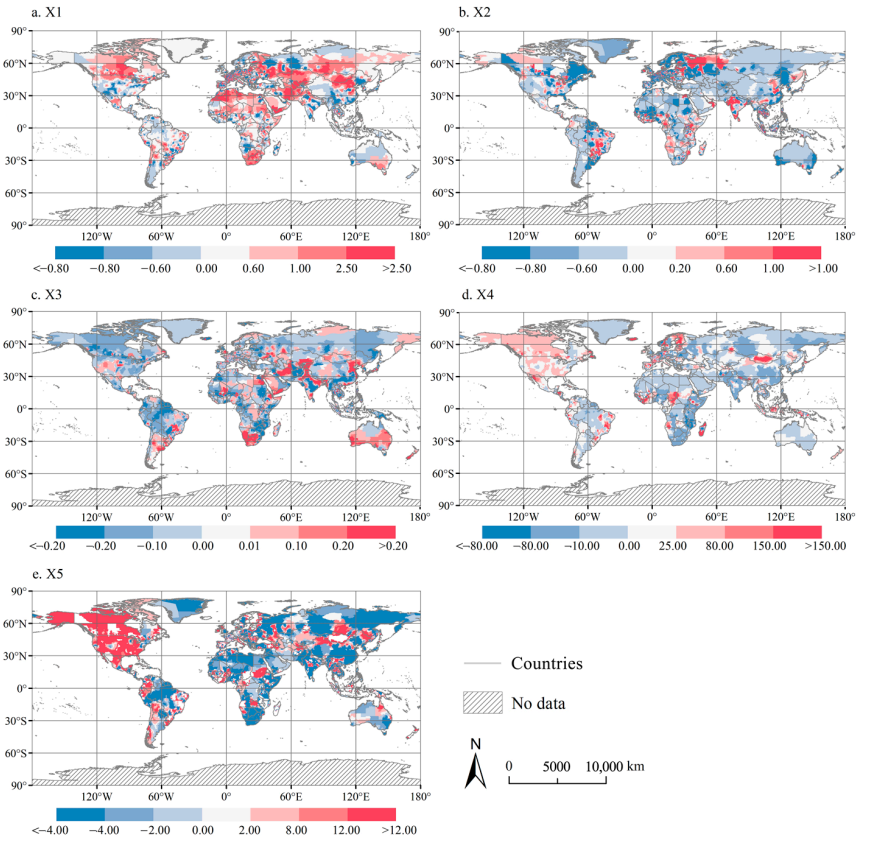


Figure 13. Coefficients of GWR model in 2020.

Altitude had a negative impact on the global CCD of the PLES functional index on a global scale. Most regions were covered by negative impact areas and only some scattered positive impact areas were distributed in various regions of the world (e.g., northern Europe, areas surrounding Africa, Brazil in South America, and parts of North America). These results indicated that the CCD of the global PLES functional index decreased with increasing altitude. Similarly, there was little overall change in the regional positive impact of altitude on the CCD of the global PLES functional index in 2010 and 2020. In contrast, areas with positive impacts increased in 2010 and 2020, but areas with negative impacts remained dominant. The proportion of forest positively affected the CCD of the global PLES functional index. In 2000, the positive impact areas were mainly observed in southern Australia, western China, North China Plain, Central Asia, and parts of South Asia, and they were scattered in other areas. The negative effects of nighttime light density on CCD of the global PLES functional index were larger than the positive effects. The most significant negative effects were found in North China. Eurasia, South America, and Africa showed an overall negative effect, but there were a few sporadic positive effects with high values clustered in Western Europe and Central Asia in Afghanistan and Georgia. In addition, North America as a whole showed a weak positive effect. The influence of the road density on the CCD of the global PLES functional index was generally negative; however, the regional distribution of the positive influence was also extensive. Positive influence areas were primarily located in North and South America, Africa, parts of Europe (southern Russia), Central Asia, Mongolia, Inner Mongolia in China, and southeastern Australia.

4. Discussion

4.1. Spatial Evolution Rules of Global PLES

Using global PLES data, this study demonstrated that global PLES has undergone significant spatiotemporal evolution. PLES evolution has become increasingly complex due to intensifying global climate change, including the increasing frequency of extreme climate events, grassland and forest degradation in many areas, wetland reduction, desertification, and soil erosion [57–61]. While ES occupied the dominant proportion and LS the smallest, significant changes in global PLES were observed during the study period. PS and LS showed a trend of continuous increase, while ES showed a trend of continuous reduction. The spatial distribution of PS in developed and developing countries was completely different. The PS of developed countries was primarily concentrated in a few economically developed cities and regions, forming industrial clusters and parks. In developing countries, due to differences in resource endowment and economic development level, the spatial distribution of PS was relatively dispersed, mainly in the form of agricultural production and primary industry, with industrialization leading to the formation of new PS growth points. With the acceleration of global urbanization, LS gradually moved from rural to urban areas, with the urban areas becoming the hub for the population and socioeconomic activities. Simultaneously, with the development of transportation and communication technology, the connections between cities have become closer, forming metropolitan areas, and the diffusion effect of LS has become increasingly prominent. This study found that the ES was under tremendous pressure. On a global scale, some countries and regions have recognized the importance of ecological protection and begun to take measures to protect ES, such as setting up nature reserves and ecological red lines.

The overall PS and LS decreased gradually with increasing altitude, while that of ES increased. Similarly, the total PS and LS gradually decreased with increasing slope, whereas that of ES gradually increased. In 2000, 2010, and 2020, the proportions of PS at altitudes greater than 2000 m were 0.894%, 0.869%, and 1.043%, and those of LS were 1.076%, 0.731%, and 0.940%, respectively. In addition, in 2000, 2010, and 2020, the proportions of PS with slopes greater than 25° were 3.540%, 3.530%, and 3.670%, and those of LS were 1.410%, 1.590%, and 1.820%, respectively. PS and LS demonstrated clear trends of expansion into the highlands. The proportion of global ES in high-altitude and high-slope areas decreased in 2000, 2010, and 2020. Previous studies demonstrated that human activities

have an apparent trend of expanding to the highlands and ES has been occupied in large quantities [58,62–65].

The global scopes of PS and LS were similar but that of PS was broader than that of LS. ES covers a vast area and most of the world is dominated by ecological functions. As the world continues to industrialize and urbanize at a rapid pace, the spatial structure of the territory has undergone significant changes and its impact on the ecological environment has been increased over time. The resulting environmental problems have also intensified, leading to decreases in ESI [61,66,67]. Areas with a relatively high degree of functional CCD of PLES were primarily distributed in the agglomeration areas of human activities. These areas were densely populated areas of surface population, economy, and industry, and were among the most complex areas in terms of the interaction between human activity and natural ecosystems. They were also important regions that needed to coordinate the contradiction between regional development and protection to achieve sustainable socioeconomic development [68].

4.2. Driving Mechanism of Global PLES Functional Index

The impact of various selected factors on the CCD of the global PLES functional index demonstrated considerable spatial variation. Global topography is complex and diverse, and climate and vegetation succession differ in latitude and longitude; thus, the regional spatial pattern of PLES showed noticeable regional differences. The impacts of terrain and climatic factors on the CCD of the PLES functional index are spatially heterogeneous. Physical geographical factors are the basis for the formation of global PLES spatial patterns and have an important impact on these patterns. Natural resource endowment is the natural basis that affects the CCD of the PLES functional index. Differing natural resource conditions in different regions directly affect the layout of PS, comfort of LS, and protection of ES. For example, regions rich in water resources are more likely to develop agricultural and water industries, whereas those rich in mineral resources may face greater environmental risks. The annual precipitation had a positive but weak effect on the PLES functional index CCD in most areas. On the contrary, there was a strong negative effect in the discrete regions, which explained the overall direction. This is because increased precipitation promotes the growth of vegetation and enhances ecosystem stability and resilience, thereby positively affecting ecological and productive space. Furthermore, climate change is also expected to cause significant alterations to demographic and social structures, increasing social inequality and deepening regional economic differentiation.

Socioeconomic development is the core driving force of the CCD of the PLES functional index. The industrial structure has been continuously optimized and upgraded with economic growth. The increased intensity and efficiency of PS provide more material foundation and financial support for LS and ES. Urbanization promotes the expansion of LS and the reconstruction and upgrading of PS. However, rapid urbanization is also likely to lead to urban issues such as traffic congestion and environmental pollution, affecting the quality of life and ecological safety. In addition, the level of environmental governance is an essential indicator for measuring a region's sustainable development ability, and the design of policies, regulations, and institutions has guiding and constraining effects on the CCD of the global PLES functional index.

The formation and evolution of the CCD of the global PLES functional index were characterized by complexity and dynamic changes, which were influenced by natural constraints, humanistic driving forces, and human–earth interaction forces. The factors that influence the CCD of the global PLES functional index differ by region. Therefore, scientifically revealing the spatiotemporal differentiation of the natural binding and human driving forces in the evolution of the CCD of the global PLES functional index is vital for studying and determining the development direction and evolution trend of the CCD of the global PLES functional index [45,46].

4.3. Policy Implications

With the rapid advancement of urbanization and industrialization, the coordinated development of PLES functional indices often faces the problems of imbalance and dislocation [2,8]. Through in-depth analyses of the underlying driving factors behind them, including differences in regional resource endowments, inequalities in policy support, differences in economic structures, imbalances in population distribution, etc., targeted countermeasures will be formulated to promote synergistic development among different regions.

The findings of the study indicate that economically developed regions, including the United States, European countries, parts of India and China, demonstrate superior performance in the functionally coordinated development of PLES. This is attributed to their robust economic foundations and abundant resource endowments. In contrast, less developed regions encounter significant challenges, including a scarcity of resources and inadequate infrastructure, which impedes the coordinated functional development of PLES and hinders the potential for synergistic effects. This uneven development impedes the attainment of sustainable development and constitutes an impediment to the objective of global synergistic development.

At the eco-environment level, it is necessary to strengthen the ecological protection and restoration work and establish a perfect ecological compensation mechanism and environmental governance system to promote the harmonious symbiosis of the eco-environment, economy, and social development [68–70]. Meanwhile, it is necessary to accelerate the adjustment of industrial structure, promote the development of a green economy and circular economy, and achieve the efficient use of resources and recycling to achieve the balanced development of economic, social, and ecological benefits [71]. At the level of social progress, it is necessary to pay attention to social equity and livelihood protection; promote the coordinated development of education, health, employment, and other social undertakings; and promote harmonious social progress by improving people's livelihoods to provide support for sustainable socioeconomic development.

In addition, promoting the coordinated development of the PLES functional index requires the joint efforts of the government, enterprises, and all sectors of society. The government should increase policy support, guide and encourage enterprises to strengthen environmental protection investment, promote industrial structure upgrading, and improve the efficiency of resource utilization. The enterprises should strengthen the awareness of social responsibility, and actively participate in environmental protection and social welfare. The public need to enhance environmental protection awareness and actively participate in public welfare activities so as to contribute to the harmony and stability of society.

Finally, in response to climate change, it is crucial to support the research, development, and application of clean energy, energy conservation and emission reduction, and green manufacturing technologies. Strengthening international technological cooperation, especially technology transfer to developing countries, is vital to global green development. The international community should improve the ecological governance framework and share the fruits of green development. Countries should sign and implement environmental protection conventions, and international cooperation should be pursued to address the environmental crisis and achieve global sustainable development.

4.4. Validity and Uncertainty

It should be noted that the evaluation results were subjective to some extent and future research needs to further quantify and objectify the spatiotemporal characteristics of the PLES function. The scoring criteria system of PLES in this study is primarily used in the Chinese study area and expert knowledge, which may have an impact on the global generalizability of this scoring system, and this study aimed to explore the extension of the concept of PLES globally with the aim of revealing the driving forces of the global CCD of the PLES function. In future studies, we will consider improvements to the scoring system to enhance its generalizability. In research on the CCD of the PLES function, the selection of the driving factors is critical. To better understand and solve the problem of

the CCD of the PLES function, we need to strengthen the monitoring and analysis system construction of the driving factors. This includes establishing a perfect monitoring network and database, collecting and sorting out the data of numerous factors affecting the CCD of the PLES function, and using modern technical means for data analysis and modeling. In addition, while this study explored the factors affecting the CCD of PLES functions from multiple dimensions, such as nature and social economy, it did not cover all the key variables owing to data accessibility and the complexity of model construction. Future studies should further expand the research scope of the influencing factors, include more complex variables, build a more comprehensive and systematic analysis framework, and deepen our understanding of the CCD of PLES functions.

5. Conclusions

This study revealed the spatial heterogeneity of the drivers of the CCD of global county-scale PLES functions in 2000, 2010, and 2020 using the CCD and GWR models. Approximately 85% of the world was dominated by ES, followed by PS (13%) and LS (3%). Topographic factors were the main factors restricting PLES. With an increase in altitude and slope, the proportions of PS and LS gradually decreased, whereas that of ES gradually increased. PS and LS demonstrated clear trends of expansion into the highlands. The functional indices of PS and LS were mainly distributed in the human activity gathering areas and a large area was covered by ES. The CCD results showed that the CCD of global PLES functions showed a gradually increasing trend, increasing from 0.186 in 2020 to 0.198 in 2020. The high-value area of the CCD was mainly distributed in the area where the interaction between the human and natural systems was relatively intense. The formation of the CCD of the global PLES functional pattern was the result of the joint action of natural and socioeconomic factors and showed evident spatial heterogeneity. This study provided a possible research path for the realization of global SDGs. Different countries and regions have different experiences and lessons in the management and utilization of PLES. Through a comparative analysis of successful and failed cases in different countries and regions, this study provided a useful reference and inspiration for other countries and regions to promote healthy and sustainable development in the global urbanization process.

Author Contributions: Conceptualization, W.L. and Y.Z.; methodology, W.L., Y.C. and Y.Z.; software, W.L., Y.Z. and W.C.; resources, Y.Z. and W.C.; data curation, Y.D. and Y.P.; writing—original draft, W.L. and Y.Z.; writing—review and editing, Z.Y. and Y.D.; supervision, W.L. and W.C. All authors have read and agreed to the published version of the manuscript.

Funding: This research was supported by the Humanities and Social Sciences Research Projects of the Provincial Department of Education [Grant No. 23Q170, No. 22Q160] and the Youth Scientific Research Fund Project of Hubei University of Economics [Grant No. XJYB202309].

Data Availability Statement: The original contributions presented in the study are included in the article, further inquiries can be directed to the corresponding author.

Conflicts of Interest: The authors declare no conflicts of interest.

References

1. Wang, Y.; Liu, X.L.; Wei, X.; Yu, H. The method and practice of regional spatial planning: From "three living Spaces" to "three districts and three lines". *J. Urban. Plan* **2018**, *4*, 65–74.
2. Li, J.S.; Sun, W.; Li, M.Y.; Meng, L.L. Coupling coordination degree of production, living and ecological spaces and its influencing factors in the Yellow River Basin. *J. Clean. Prod.* **2021**, *298*, 126803. [CrossRef]
3. Song, W.; Cao, S.S.; Du, M.Y.; He, Z.Y. Aligning territorial spatial planning with sustainable development goals: A comprehensive analysis of production, living, and ecological spaces in China. *Ecol. Indic.* **2024**, *160*, 111816. [CrossRef]
4. Zhang, L.D.; Hou, Q.H.; Duan, Y.Q. Under the background of ecological civilization grow space research: The connotation, development and countermeasures. *Acta Ecol. Sin.* **2024**, *44*, 47–59.
5. Billaud, O.; Soubeyrand, M.; Luque, S.; Lenormand, M. Comprehensive decision-strategy space exploration for efficient territorial planning strategies. *Comput. Environ. Urban Syst.* **2020**, *83*, 101516. [CrossRef]
6. Bai, R.; Shi, Y.; Pan, Y. Land-use classifying and identification of the production-living-ecological space of island villages–a case study of islands in the western sea area of Guangdong Province. *Land* **2022**, *11*, 705. [CrossRef]

7. Chen, H.J.; Yang, Q.Y.; Su, K.C.; Zhang, H.Z.; Lu, D.; Xiang, H.; Zhou, L.L. Identification and optimization of production-living-ecological space in an ecological foundation area in the upper reaches of the yangtze river: A case study of jiangjin district of Chongqing, China. *Land* **2021**, *10*, 863. [CrossRef]
8. Fu, J.Y.; Gao, Q.; Jiang, D.; Li, X.; Lin, G. Spatial–temporal distribution of global production-living-ecological space during the period 2000–2020. *Sci. Data* **2023**, *10*, 589. [CrossRef]
9. Li, Y.P.; Zhang, S.Q.; Zhao, J.S.; Zhang, G.R.; Qu, G.X.; Ma, S.L.; Liu, X.B. Spatiotemporal evolution and sustainably comprehensive zoning optimization of production-living-ecological functions in the Mountain–Flatland areas. *Heliyon* **2024**, *10*, e23425. [CrossRef]
10. Wang, J.Y.; Sun, Q.; Zou, L.L. Spatial-temporal evolution and driving mechanism of rural production-living-ecological space in Pingtan islands, China. *Habitat Int.* **2023**, *137*, 102833. [CrossRef]
11. Ji, Z.X.; Liu, C.; Xu, Y.Q.; Sun, M.X.; Wei, H.J.; Sun, D.F.; Li, Y.Y.; Zhang, P.; Sun, Q.Q. Quantitative identification and the evolution characteristics of production-living-ecological space in the mountainous area: From the perspective of multifunctional land. *J. Geogr. Sci.* **2023**, *33*, 779–800. [CrossRef]
12. Xia, N.; Hai, W.Y.; Tang, M.Y.; Song, J.M.; Quan, W.L.; Zhang, B.W.; Ma, Y.G. Spatiotemporal evolution law and driving mechanism of production-living-ecological space from 2000 to 2020 in Xinjiang, China. *Ecol. Indic.* **2023**, *154*, 110807. [CrossRef]
13. Zhao, J.; Zhao, Y.L. Synergy/trade-offs and differential optimization of production, living, and ecological functions in the Yangtze River economic Belt, China. *Ecol. Indic.* **2023**, *147*, 109925. [CrossRef]
14. Deng, Y.X.; Yang, R. Influence mechanism of production-living-ecological space changes in the urbanization process of Guangdong Province, China. *Land* **2021**, *10*, 1357. [CrossRef]
15. Tao, Y.Y.; Wang, Q.X. Quantitative recognition and characteristic analysis of production-living-ecological space evolution for five resource-based cities: Zululand, Xuzhou, Lota, Surf Coast and Ruhr. *Remote Sens.* **2021**, *13*, 1563. [CrossRef]
16. Aizizi, Y.; Kasimu, A.; Liang, H.; Zhang, X.; Zhao, Y.; Wei, B. Evaluation of ecological space and ecological quality changes in urban agglomeration on the northern slope of the Tianshan Mountains. *Ecol. Indic.* **2023**, *146*, 109896. [CrossRef]
17. Abe, Y.; Yamada, K.; Tanaka, R.; Ando, K.; Ueno, M. Dynamic living space: Toward a society where people can live anywhere in 2050. *Futures* **2024**, *161*, 103363. [CrossRef]
18. Liu, Y.Y.; Liu, X.Y.; Zhao, C.Y.; Wang, H.; Zang, F. The trade-offs and synergies of the ecological-production-living functions of grassland in the Qilian mountains by ecological priority. *J. Environ. Manag.* **2023**, *327*, 116883. [CrossRef]
19. Feng, C.C.; Zhang, H.; Xiao, L.; Guo, Y.P. Land use change and its driving factors in the rural–urban fringe of Beijing: A production-living-ecological perspective. *Land* **2022**, *11*, 314. [CrossRef]
20. Jiang, X.T.; Zhai, S.Y.; Liu, H.; Chen, J.; Zhu, Y.Y.; Wang, Z. Multi-scenario simulation of production-living-ecological space and ecological effects based on shared socioeconomic pathways in Zhengzhou, China. *Ecol. Indic.* **2022**, *137*, 108750. [CrossRef]
21. Liao, G.T.; He, P.; Gao, X.S.; Lin, Z.Y.; Huang, C.Y.; Zhou, W.; Deng, O.P.; Xu, C.H.; Deng, L.J. Land use optimization of rural production-living-ecological space at different scales based on the BP–ANN and CLUE–S models. *Ecol. Indic.* **2022**, *137*, 108710. [CrossRef]
22. Wang, D.; Fu, J.Y.; Jiang, D. Optimization of production-living-ecological space in national key poverty-stricken city of southwest China. *Land* **2022**, *11*, 411. [CrossRef]
23. Wang, L.L.; Zhou, S.J.; Ouyang, S.Y. The spatial prediction and optimization of production-living-ecological space based on Markov–PLUS model: A case study of Yunnan Province. *Open Geosci.* **2022**, *14*, 481–493. [CrossRef]
24. Wu, J.S.; Zhang, D.N.; Wang, H.; Li, X.C. What is the future for production-living-ecological spaces in the Greater Bay Area? A multi-scenario perspective based on DEE. *Ecol. Indic.* **2021**, *131*, 108171. [CrossRef]
25. Zhang, Y.; Zheng, M.R.; Qin, B. Optimization of spatial layout based on ESV-FLUS model from the perspective of "Production-Living-Ecological": A case study of Wuhan City. *Ecol. Model.* **2023**, *481*, 110356. [CrossRef]
26. Mohammadyari, F.; Tavakoli, M.; Zarandian, A.; Abdollahi, S. Optimization land use based on multi-scenario simulation of ecosystem service for sustainable landscape planning in a mixed urban-Forest watershed. *Ecol. Model.* **2023**, *483*, 110440. [CrossRef]
27. Lark, T.J.; Spawn, S.A.; Bougie, M.; Gibbs, H.K. Cropland expansion in the United States produces marginal yields at high costs to wildlife. *Nat. Commun.* **2020**, *11*, 4295. [CrossRef]
28. Wang, A.Y.; Liao, X.Y.; Tong, Z.J.; Du, W.L.; Zhang, J.Q.; Liu, X.P.; Liu, M.S. Spatial-temporal dynamic evaluation of the ecosystem service value from the perspective of "production-living-ecological" spaces: A case study in Dongliao River Basin, China. *J. Clean. Prod.* **2022**, *333*, 130218. [CrossRef]
29. Li, C.X.; Wu, J.Y. Land Use Transformation and eco-environmental effects based on production-living-ecological spatial synergy: Evidence from Shaanxi Province, China. *Environ. Sci. Pollut. Res.* **2022**, *29*, 41492–41504. [CrossRef]
30. Pang, R.Q.; Hu, N.; Zhou, J.R.; Sun, D.Q.; Ye, H.Y. Study on eco-environmental effects of land-use transitions and their influencing factors in the Central and Southern Liaoning Urban Agglomeration: A production-living-ecological perspective. *Land* **2022**, *11*, 937. [CrossRef]
31. Yang, Y.Y.; Bao, W.K.; Liu, Y.S. Coupling coordination analysis of rural production-living-ecological space in the Beijing-Tianjin-Hebei region. *Ecol. Indic.* **2020**, *117*, 106512. [CrossRef]
32. Cheng, Z.L.; Zhang, Y.J.; Wang, L.Z.; Wei, L.Y.; Wu, X.Y. An analysis of land-use conflict potential based on the perspective of production-living-ecological function. *Sustainability* **2022**, *14*, 5936. [CrossRef]

33. Ntakana, K.; Mbanga, S.; Botha, B.; Ariyan, L. Inclusive urban space production model for sustainable development in South Africa. *Heliyon* **2023**, *9*, e16391. [CrossRef] [PubMed]
34. Zou, L.L.; Liu, Y.S.; Wang, J.Y.; Yang, Y.Y. An analysis of land use conflict potentials based on ecological-production-living function in the southeast coastal area of China. *Ecol. Indic.* **2021**, *122*, 107297. [CrossRef]
35. Leng, A.; Wang, K.; Bai, J.J.; Gu, N.; Feng, R.T. Analyzing sustainable development in Chinese cities: A focus on land use efficiency in production-living-ecological aspects. *J. Clean. Prod.* **2024**, *448*, 141461. [CrossRef]
36. Yu, S.H.; Deng, W.; Xu, Y.X.; Zhang, X.; Xiang, H.L. Evaluation of the production-living-ecology space function suitability of Pingshan County in the Taihang mountainous area, China. *J. Mt. Sci.* **2020**, *17*, 2562–2576. [CrossRef]
37. Zhang, X.S.; Xu, Z.J. Functional coupling degree and human activity intensity of production-living-ecological space in underdeveloped regions in China: Case study of Guizhou Province. *Land* **2021**, *10*, 56. [CrossRef]
38. Duan, Y.M.; Wang, H.; Huang, A.; Xu, Y.Q.; Lu, L.H.; Ji, Z.X. Identification and spatial-temporal evolution of rural "production-living-ecological" space from the perspective of villagers' behavior—A case study of Ertai Town, Zhangjiakou City. *Land Use Policy* **2021**, *106*, 105457. [CrossRef]
39. Fu, J.Y.; Bu, Z.Q.; Jiang, D.; Lin, G.; Li, X. Sustainable land use diagnosis based on the perspective of production-living-ecological spaces in China. *Land Use Policy* **2022**, *122*, 106386. [CrossRef]
40. Wei, L.Y.; Zhang, Y.J.; Wang, L.Z.; Mi, X.Y.; Wu, X.Y.; Cheng, Z.L. Spatiotemporal evolution patterns of "production-living-ecological" spaces and the coordination level and optimization of the functions in Jilin Province. *Sustainability* **2021**, *13*, 13192. [CrossRef]
41. Yang, D.R.; Yang, Q.; Tong, Z.J.; Du, W.L.; Zhang, J.Q. Coupling coordination analysis of production, living, and ecological spaces in wetlands: A case study of Xianghai Wetland nature reserve, China. *Ecol. Indic.* **2024**, *158*, 111578. [CrossRef]
42. Gao, Y.; Bai, L.; Zhou, K.; Kou, Y.; Yuan, W.; Zhou, X.; Qiu, Z.; Zhao, D.; Lv, Z.; Wu, Q.; et al. Study on the Coupling Coordination Degree and Driving Mechanism of "Production-Living-Ecological" Space in Ecologically Fragile Areas: A Case Study of the Turpan–Hami Basin. *Sustainability* **2024**, *16*, 9054. [CrossRef]
43. McLeman, R.; Smit, B. Migration as an adaptation to climate change. *Clim. Chang.* **2006**, *76*, 31–53. [CrossRef]
44. Hsiang, S.M.; Burke, M.; Miguel, E. Quantifying the influence of climate on human conflict. *Science.* **2013**, *341*, 1235367. [CrossRef] [PubMed]
45. Cui, X.H.; Xu, N.; Chen, W.X.; Wang, G.Z.; Liang, J.L.; Pan, S.P.; Duan, B.Q. Spatio-temporal variation and influencing factors of the coupling coordination degree of production-living-ecological space in China. *Int. J. Environ. Res. Public Health* **2022**, *19*, 10370. [CrossRef]
46. Xu, N.; Chen, W.X.; Pan, S.P.; Liang, J.L.; Bian, J.J. Evolution characteristics and formation mechanism of production-living-ecological space in China: Perspective of main function zones. *Int. J. Environ. Res. Public Health* **2022**, *19*, 9910. [CrossRef]
47. Song, Y.Y.; Xue, D.Q.; Xia, S.Y.; Mi, W.B. Characteristics and formation mechanism of territorial spatial pattern in the Yellow River Basin during the last 40 years. *Geogr. Res.* **2021**, *40*, 1445–1463.
48. Wang, Q.; Wang, H.J. Dynamic simulation and conflict identification analysis of production-living-ecological space in Wuhan, Central China. *Integr. Environ. Assess. Manag.* **2022**, *18*, 1578–1596. [CrossRef]
49. Kong, D.Y.; Chen, H.G.; Wu, K.S. The evolution of "Production-Living-Production" space eco-environmental effects and its influencing factors in China. *J. Nat. Resour.* **2021**, *36*, 1116–1135. [CrossRef]
50. Dong, Z.H.; Zhang, J.Q.; Si, A.; Tong, Z.J.; Na, L. Multidimensional analysis of the spatiotemporal variations in ecological, production and living spaces of Inner Mongolia and an identification of driving forces. *Sustainability* **2020**, *12*, 7964. [CrossRef]
51. Cui, J.X.; Gu, J.; Sun, J.W.; Luo, J. The spatial pattern and evolution characteristics of the production, living and ecological space in Hubei Provence. *China Land Sci.* **2018**, *32*, 67–73.
52. Liu, J.L.; Liu, Y.S.; Li, Y.R. Classification evaluation and spatial-temporal pattern analysis of 'three living spaces' in China. *J. Geogr.* **2017**, *72*, 1290–1304.
53. Yuill, R.S. The standard deviational ellipse; an updated tool for spatial description. *Geogr. Ann. Ser. B Hum. Geogr.* **1971**, *53*, 28–39. [CrossRef]
54. Han, D.; Yu, D.; Qiu, J. Assessing coupling interactions in a safe and just operating space for regional sustainability. *Nat. Commun.* **2023**, *14*, 1369. [CrossRef]
55. Anselin, L. A test for spatial autocorrelation in seemingly unrelated regressions. *Econ. Lett.* **1988**, *28*, 335–341. [CrossRef]
56. Charlton, M.E.; Brunsdon, C.F.; Fotheringham, A.S. Geographically weighted regression-modelling spatial non-stationarity. *Am. Stat.* **1998**, *47*, 431–443.
57. Winkler, K.; Fuchs, R.; Rounsevell, M.; Herold, M. Global land use changes are four times greater than previously estimated. *Nat. Commun.* **2021**, *12*, 2501. [CrossRef]
58. Mousivand, A.; Arsanjani, J.J. Insights on the historical and emerging global land cover changes: The case of ESA-CCI-LC datasets. *Appl. Geogr.* **2019**, *106*, 82–92. [CrossRef]
59. Ma, J.; Li, J.W.; Wu, W.B.; Liu, J.J. Global forest fragmentation change from 2000 to 2020. *Nat. Commun.* **2023**, *14*, 3752. [CrossRef]
60. Potapov, P.; Turubanova, S.; Hansen, M.C.; Tyukavina, A.; Zalles, V.; Khan, A.; Song, X.-P.; Pickens, A.; Shen, Q.; Cortez, J. Global maps of cropland extent and change show accelerated cropland expansion in the twenty-first century. *Nat. Food* **2022**, *3*, 19–28. [CrossRef]

61. Li, G.D.; Fang, C.L.; Li, Y.J.; Wang, Z.B.; Sun, S.; He, S.W.; Qi, W.; Bao, C.; Ma, H.T.; Fan, Y.J.; et al. Global impacts of future urban expansion on terrestrial vertebrate diversity. *Nat. Commun.* **2022**, *13*, 1628. [CrossRef] [PubMed]
62. Meng, Z.Q.; Dong, J.W.; Ellis, E.C.; Metternicht, G.; Qin, Y.W.; Song, X.P.; Löfqvist, S.; Garrett, R.; Jia, X.P.; Xiao, X.M. Post-2020 biodiversity framework challenged by cropland expansion in protected areas. *Nat. Sustain.* **2023**, *6*, 758–768. [CrossRef]
63. Van Vliet, J. Direct and indirect loss of natural area from urban expansion. *Nat. Sustain.* **2019**, *2*, 755–763. [CrossRef]
64. Yang, C.; Liu, H.Z.; Li, Q.Q.; Wang, X.Q.; Ma, W.; Liu, C.L.; Fang, X.; Tang, Y.Z.; Shi, T.Z.; Wang, Q.B.; et al. Human expansion into Asian highlands in the 21st Century and its effects. *Nat. Commun.* **2022**, *13*, 4955. [CrossRef] [PubMed]
65. Zeng, Z.; Estes, L.; Ziegler, A.D.; Chen, A.; Searchinger, T.; Hua, F.; Guan, K.; Jintrawet, A.; Wood, E.F. Highland cropland expansion and forest loss in Southeast Asia in the twenty-first century. *Nat. Geosci.* **2018**, *11*, 556–562. [CrossRef]
66. Das, M.; Das, A.; Pereira, P. Impact of urbanization induced land use and land cover change on ecological space quality-mapping and assessment in Delhi (India). *Urban Clim.* **2024**, *53*, 101818. [CrossRef]
67. Das, A.; Das, M. Exploring the relationship between quality of living and green spaces in cities: Evidence from an Indian megacity region of global south. *Land Use Policy* **2023**, *129*, 106594. [CrossRef]
68. Knight, S.J.; McClean, C.J.; White, P.C.L. The importance of ecological quality of public green and blue spaces for subjective well-being. *Landsc. Urban Plan* **2022**, *226*, 104510. [CrossRef]
69. Pan, S.P.; Chen, W.X.; Liang, J.L.; Li, J.F. Comparison of domestic and international spatial planning research based on bibliometric analysis. *China Agric. Resour. Zoning* **2023**, *44*, 131–144.
70. Liu, Y.X.; Fu, B.J.; Wang, S.; Rhodes, J.R.; Li, Y.; Zhao, W.; Li, C.J.; Zhou, S.; Wang, C.X. Global assessment of nature's contributions to people. *Sci. Bull.* **2023**, *68*, 424–435. [CrossRef]
71. Aguilar, A.G.; Hernandez-Lozano, J. Mega-urbanization, territorial fragmentation and social inequality in the Global South: The case of Mexico city and its city-region. *Appl. Geogr.* **2024**, *163*, 103183. [CrossRef]

Disclaimer/Publisher's Note: The statements, opinions and data contained in all publications are solely those of the individual author(s) and contributor(s) and not of MDPI and/or the editor(s). MDPI and/or the editor(s) disclaim responsibility for any injury to people or property resulting from any ideas, methods, instructions or products referred to in the content.